

Response of the C4 magnetic phase in iron-based superconductors to electronic structure tuning via doping/uniaxial strain

Li-Li Meng(孟丽丽), Ting-Ting Han(韩婷婷), Yu-Jing Ren(任宇靖), Jing-Zhi Chen(陈景芝), Peng-Hao Yuan(袁鹏浩), and Yan Zhang(张焱)

Citation: Chin. Phys. B, 2026, 35 (**5**): 057404. DOI: 10.1088/1674-1056/ae3c8e
http://cpb.iphy.ac.cn; http://iopscience.iop.org/cpb

What follows is a list of articles you may be interested in

Crystal growth and characterization of a hole-doped iron-based superconductor $Ba(Fe_{0.875}Ti_{0.125})_2As_2$

Yi-Li Sun(孙毅丽), Ze-Zhong Li(李泽众), Yang Li(李阳), Hong-Lin Zhou(周宏霖), Amit Pokhriyal, Haranath Ghosh, Shi-Liang Li(李世亮), and Hui-Qian Luo(罗会仟)

Chin. Phys. B, 2025, 34 (**12**): 127401. DOI: 10.1088/1674-1056/ae0d5a

Surface reconstruction modulated superconductivity on quasi-2D iron pnictide superconductor $KCa_2Fe_4As_4F_2$

Wenjing Zeng(曾文静), Zongyuan Zhang(张宗源), Xiaoyan Dong(董晓燕), Yubing Tu(涂玉兵), Yanwei Wu(吴彦玮), Teng Wang(王腾), Fan Zhang(张凡), Shuai Shao(邵帅), Jie Hou(侯杰), Xingyuan Hou(侯兴元), Ning Hao(郝宁), Gang Mu(牟刚), and Lei Shan(单磊)

Chin. Phys. B, 2025, 34 (**8**): 087402. DOI: 10.1088/1674-1056/add5cb

Dimensional crossover from quasi-2D to 3D superconductivity in $(Li,Fe)OHFeSe_{1-x}S_x$ driven by chemical pressure

Yuxin Ma(马宇欣), Munan Hao(郝木难), Qi Li(李琦), Ke Ma(马克), Haodong Li(李浩东), Duo Zhang(张铎), Ruijin Sun(孙瑞锦), Shifeng Jin(金士锋), and Changchun Zhao(赵长春)

Chin. Phys. B, 2025, 34 (**6**): 067402. DOI: 10.1088/1674-1056/adc404

Co-doped $BaFe_2As_2$ Josephson junction fabricated with a focused helium ion beam

Ziwen Chen(陈紫雯), Yan Zhang(张焱), Ping Ma(马平), Zhongtang Xu(徐中堂), Yulong Li(李宇龙), Yue Wang(王越), Jianming Lu(路建明), Yanwei Ma(马衍伟), and Zizhao Gan(甘子钊)

Chin. Phys. B, 2024, 33 (**4**): 047405. DOI: 10.1088/1674-1056/ad21f7

Focused-ion-beam assisted technique for achieving high pressure by uniaxial-pressure devices

Di Liu(刘迪), Xingyu Wang(王兴玉), Zezhong Li(李泽众), Xiaoyan Ma(马肖燕), and Shiliang Li(李世亮)

Chin. Phys. B, 2023, 32 (**4**): 047401. DOI: 10.1088/1674-1056/acac1a

---

RAPID COMMUNICATION

Response of the C4 magnetic phase in iron-based superconductors to electronic structure tuning via doping/uniaxial strain

Li-Li Meng(孟丽丽)[1], Ting-Ting Han(韩婷婷)[1], Yu-Jing Ren(任宇靖)[1], Jing-Zhi Chen(陈景芝)[1], Peng-Hao Yuan(袁鹏浩)[1], and Yan Zhang(张焱)[1,2,†]

[1] *International Center for Quantum Materials, School of Physics, Peking University, Beijing* 100871, *China*
[2] *Collaborative Innovation Center of Quantum Matter, Beijing* 100871, *China*

(Received 28 November 2025; revised manuscript received 20 January 2026; accepted manuscript online 23 January 2026)

Elucidating how magnetic interactions are established in high-temperature superconductors is crucial for resolving the long-standing puzzle of the superconducting pairing mechanism. However, for iron-based superconductors, due to the diversity of their magnetic and electronic structures, the mechanism of magnetic interactions remains controversial. Here, we employed *in-situ* alkali-metal deposition and uniaxial strain to tune the four-fold (C4) magnetic phase in $Sr_{0.64}Na_{0.36}Fe_2As_2$ and utilized angle-resolved photoemission spectroscopy (ARPES) to probe the response of its electronic structure. We found that the alkali-metal deposition suppresses the C4 magnetic phase effectively, driving the system into a stripe spin density wave phase with two-fold rotational (C2) symmetry. Counterintuitively, the uniaxial strain that naturally breaks the C4 rotational symmetry of the lattice exerts only a limited suppressive effect on the C4 magnetic phase. While the sensitivity of C4 magnetic phase to electron doping implies that the orbital selectivity of Fermi surface nesting plays a critical role in determining the magnetic configuration, validating the contribution of itinerant electrons in mediating the magnetic fluctuations, the insensitivity of the C4 magnetic phase to uniaxial strain suggests that the nematic order exhibits no intermediate correlation with the magnetism in iron-based superconductors. Our results provide crucial clues for a comprehensive understanding of the complex phase diagram of iron-based superconductors.

Keywords: iron-based superconductors, angle-resolved photoemission spectroscopy, spin density wave

PACS: 74.70.Xa, 79.60.–i, 74.25.Jb, 75.30.Fv

DOI: 10.1088/1674-1056/ae3c8e **CSTR:** 32038.14.CPB.ae3c8e

1. Introduction

In the research of high-temperature superconductors (HTS),[1–4] it has been found that the superconducting phase is always intertwined with magnetic phases. As magnetic phases are suppressed by either doping or pressure, magnetic fluctuations intensify and the superconducting phase emerges. Based on this general phase diagram of HTS, it is believed that the superconducting pairing mechanism is associated with magnetic fluctuations or magnetic interactions. A correct understanding of how magnetic interactions are established in the parent phase of HTS is regarded as the key to unveiling the pairing mechanism of HTS. For iron-based high-temperature superconductors (Fe-HTS), various magnetic phases with distinct periodicities and magnetic moment orientations have been identified.[4] For example, bicollinear and $\sqrt{5}\times\sqrt{5}$ antiferromagnetic orders have been observed in FeTe and FeSe-based Fe-HTS.[4–6] However, their correlations with superconductivity are still under debate. Therefore, in this paper, we focus on the magnetic phases observed in FeAs-based Fe-HTS, whose correlations with superconductivity are well established.

First, in the parent compounds of FeAs-based materials, a spin density wave (SDW) phase with two-fold rotational (C2) symmetry has been observed.[4,7,8] Neutron scattering experiments confirmed that it is a stripe spin density wave (SSDW) phase [Fig. 1(a)]. The magnetic moments are aligned within the FeAs plane with a ferromagnetic order along one direction and an antiferromagnetic order along the other direction. Subsequently, in hole-doped FeAs-based materials, a magnetic phase preserving the four-fold rotational (C4) symmetry has been identified.[9–12] Experimental and theoretical studies attributed it to a charge-spin density wave (CSDW) phase, where the magnetic moments are antiparallel and oriented along the out-of-plane direction [Fig. 1(a)]. Lately, a spin-vortex crystal (SVC) phase has been found in $CaKFe_4As_4$.[13,14] It also exhibits C4 symmetry but with the magnetic moments aligned within the FeAs plane [Fig. 1(a)]. Moreover, a C2 SDW phase potentially formed by a coupling between SSDW and SVC has been observed in a small region of the phase diagram of hole-doped Fe-HTS near the superconducting phase boundary.[15,16] Theories have also proposed the presence of more complex magnetic orders in Fe-HTS arising from the coupling of multiple magnetic orders or from magnetic orders with incommensurate periodicities.[17,18]

To understand how various magnetic orders emerge in Fe-

†Corresponding author. E-mail: yzhang85@pku.edu.cn

© 2026 Chinese Physical Society and IOP Publishing Ltd. All rights, including for text and data mining, AI training, and similar technologies, are reserved.

HTS, two scenarios have been proposed. On the one hand, the magnetic interactions may originate from the nearest-neighbor and next-nearest-neighbor exchange interactions (J_1 and J_2). When $J_2 > J_1/2$, the system tends to form a SSDW order that breaks C4 symmetry.[19,20] In other parameter spaces or when long-range exchange interactions are considered, the ground state of magnetic orders varies, resulting in the emergence of different magnetic orders. On the other hand, magnetic interactions may arise from the Fermi surface instabilities.[21,22] In the one-iron Brillouin zone, the nesting between the hole Fermi pockets at the zone center and the electron Fermi pockets at the zone boundary gives rise to the magnetic instability with $Q = (0, \pi)$ or $(\pi, 0)$. When the balance between the $(0, \pi)$ magnetic order M_1 and $(\pi, 0)$ magnetic order M_2 is disrupted, for example $|M_1| \neq 0$ and $|M_2| = 0$, the system develops a SSDW order. Conversely, when two magnetic orders are balanced ($|M_1| = |M_2|$), the system tends to form a C4 magnetic order (CSDW or SVC). Moreover, a nematic transition has been found in Fe-HTS which precedes the magnetic transition in the phase diagram. Therefore, orbital instabilities arising from the multi-orbital electronic structures of Fe-HTS have also been considered as a driving force of the magnetism.[23,24] The development of different orbital or bond orders has been proposed to be crucial in determining the magnetic configurations in Fe-HTS.[25]

One approach to investigating the origin of magnetism in Fe-HTS is to tune materials via chemical doping or pressure and characterize how magnetic phases respond to various tuning parameters. However, normal tuning methods are limited by poor continuity and difficulties in integrating with high-precision spectroscopic measurements. Here, we employed two *in-situ* tuning methods, alkali-metal deposition and uniaxial strain tuning, which are compatible with angle-resolved photoemission spectroscopy (ARPES). Surface deposition of alkali metals directly dopes electrons into the sample surface, thereby regulating the surface electronic states of materials.[26,27] The uniaxial strain tuning technique based on piezoelectric ceramic stacks could continuously apply tensile or compressive strain to materials, which naturally breaks the C4 rotational symmetry of the lattice and induces anisotropy in the electronic band structure of materials.[28–30]

We focused on the CSDW phase in hole-doped $Sr_{1-x}Na_xFe_2As_2$.[12,31] In the phase diagram of $Sr_{1-x}Na_xFe_2As_2$ [Fig. 1(b)], the CSDW phase is close to the superconducting phase. Its intermediate correlation with superconductivity has been confirmed in our previous ARPES study.[31] More importantly, the CSDW phase lies in the central region of the phase diagram where the energy differences between various magnetic orders are nearly degenerate, making it ideal for investigating transitions among different magnetic phases induced by external stimuli. Here, we performed ARPES studies on $Sr_{0.64}Na_{0.36}Fe_2As_2$ tuned via alkali-metal deposition and uniaxial strain methods. We found that the alkali-metal deposition, as a method that regulates the nesting of Fermi pockets, suppresses the CSDW phase effectively. A transition from CSDW to SSDW phase was observed in the heavily electron doped samples. Our results indicate that the orbital selectivity of Fermi surface nesting plays a dominant role in determining the magnetic configuration. More specifically, in the CSDW phase, the electron pockets (e-pockets) exhibit nesting with the $d_{xz,yz}$ hole pockets (h-pockets), whereas in the SSDW phase, the nesting occurs between the e-pockets and the d_{xy} h-pocket. In the uniaxially strained samples, we found that the uniaxial strain induces a nematic order in the system with an energy scale of $\sim$ 20–30 meV. However, it only shows a limited suppression effect on the CSDW phase. No signature of the SSDW phase was observed in either tensile or compressively strained samples. This suggests that the nematic order exhibits no intermediate correlation with the magnetic order. The nematic and magnetic fluctuations may have different origins. Our experiments provide important clues for the understanding of the complex magnetism and superconductivity of Fe-HTS.

2. Method

High quality $Sr_{1-x}Na_xFe_2As_2$ ($x = 0$ and 0.36) single crystals were synthesized using the self-flux method,[12] where the doping x was determined using energy dispersive x-ray (EDX) analysis. ARPES measurements were performed at Peking University using a DA30L analyzer and a helium discharge lamp. The photon energy was 21.2 eV. The overall energy resolution was set to $\sim$ 12 meV for band structure mapping and $\sim$ 7 meV for gap measurements. The angular resolution is $\sim 0.3^\circ$. The crystals were cleaved *in-situ* and measured in ultrahigh vacuum with a base pressure better than 6×10^{-11} mbar.

The alkali-metal surface deposition was conducted *in-situ* using a lithium dispenser. We use Dn ($n = 1, 2, 3, \ldots$) to denote the doping sequence. The doping level is represented using the total deposition time. The total deposition times from D0 to D7 are around 0 s, 20 s, 40 s, 65 s, 95 s, 130 s, 175 s, 225 s respectively. The lithium coverage is estimated by counting the Fermi surface volume. The lithium coverage is estimated to be $\sim$ 0.3 ML for $\sim$ 225 s deposition time.

The uniaxial strain was applied *in-situ* using our home-made piezoelectric-based strain-tuning device, whose details can be found in Ref. [29]. The uniaxial strain was applied along the k_x direction. The strain strength was characterized by microscopy and was represented by the voltage of the piezoelectric ceramic stacks (V_{pzt}). At V_{pzt} of -300 V and 300 V, around 0.3% tensile and compressive strains could be achieved, respectively.

3. Results

3.1. Characteristics of the C2 and C4 magnetic phases

Prior to the sample manipulation, it is essential to identify the characteristics of the electronic structure in the magnetic phases with C2 and C4 symmetries. In Fig. 1, we compared the measured electronic structures in $SrFe_2As_2$ and $Sr_{0.64}Na_{0.36}Fe_2As_2$ which represent the SSDW and CSDW phases, respectively. In $SrFe_2As_2$, due to the SDW gap opening, the photoemission intensity at the Fermi energy (E_F) was strongly suppressed, we thereby plotted the photoemission intensity mapping at 40 meV below E_F to better show the different sizes of Fermi pockets. We also deposited a tiny amount of lithium on the surface of $SrFe_2As_2$ to remove the complex surface states caused by the surface polarization effect.[32] For FeAs-based Fe-HTS, there are three h-pockets at the Brillouin zone center and two e-pockets at the Brillouin zone corner.[33–35] As compared in Figs. 1(c) and 1(g), the substitution of Sr with Na introduces holes into the system, which changes the relative sizes of the h- and e-pockets. More specifically, the size of the e-pockets is comparable to the size of the d_{xy} h-pocket in $SrFe_2As_2$, but becomes closer to the size of the $d_{xz,yz}$ h-pockets in $Sr_{0.64}Na_{0.36}Fe_2As_2$.

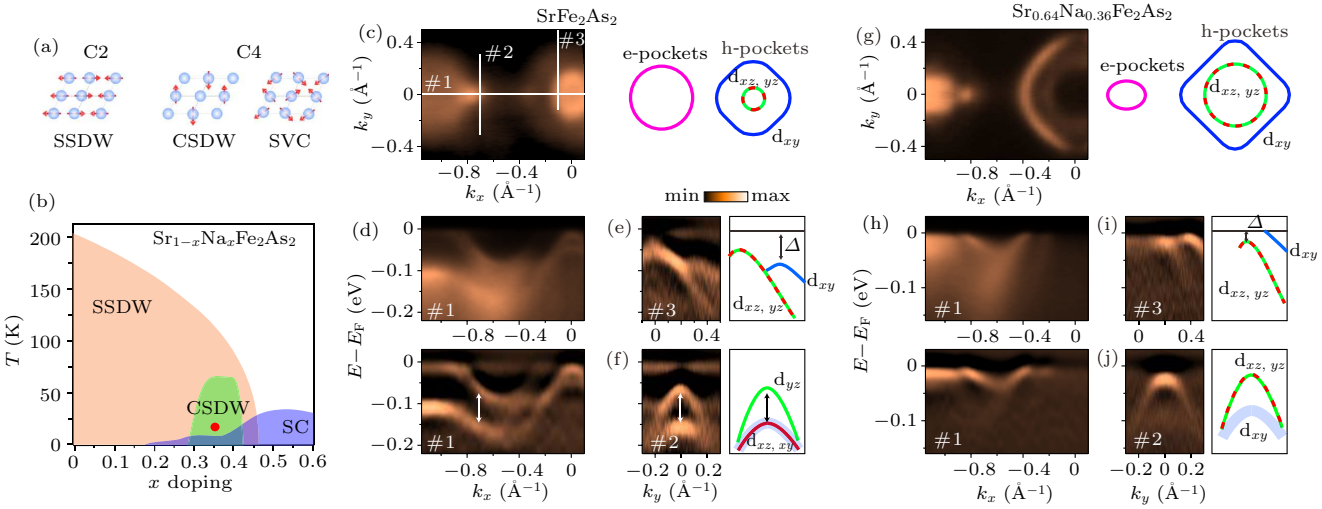


Fig. 1. Characterizations of the electronic structures of the magnetic phases with two-fold and four-fold rotational (C2 and C4) symmetries. (a) Schematic drawings of the magnetic configurations of stripe spin density wave (SSDW), charge-spin density wave (CSDW), and spin-vortex crystal (SVC) phases. (b) Phase diagram of $Sr_{1-x}Na_xFe_2As_2$. The doping level of our samples in the CSDW phase is highlighted using red circle. (c) Photoemission intensity mapping taken at 40 meV below the Fermi energy (E_F) in $SrFe_2As_2$. The schematic drawing of the electron pockets (e-pockets) and hole pockets (h-pockets) is shown in the right panel. (d) Energy momentum cuts (upper panel) and the second derivative image (bottom panel) taken along the #1 direction. (e) and (f) Second derivative images of the energy-momentum cuts and the schematic drawings of the observed band dispersions taken along the #3 and #2 directions. The cut directions are illustrated using white solid lines in panel (c). (g) Photoemission intensity mapping taken at E_F and the schematic drawing of Fermi pockets in $Sr_{0.64}Na_{0.36}Fe_2As_2$. (h)–(j) are the same as (d)–(f) but taken in $Sr_{0.64}Na_{0.36}Fe_2As_2$. The data were measured at 15 K.

When entering the SDW phases, the Brillouin zone folding results in an opening of the SDW gap near E_F. According to previous ARPES studies, such a SDW gap is orbital selective.[31,34] As shown in Fig. 1(c), the photoemission intensity of the $d_{xz,yz}$ h-pockets is much stronger than that of the d_{xy} h-pocket, indicating that the SDW gap opens primarily on the d_{xy} h-pocket in $SrFe_2As_2$. In contrast, in $Sr_{0.64}Na_{0.36}Fe_2As_2$, with the same experimental geometry, the relative intensities of the $d_{xz,yz}$ and d_{xy} h-pockets are reversed. The orbital selectivity of the SDW gap could be better visualized in the energy-momentum cuts taken along #1 and #3 directions [Figs. 1(d), 1(e), 1(h) and 1(i)]. In the SSDW phase in $SrFe_2As_2$, while the dispersion of the $d_{xz,yz}$ bands is continuous and parabolic-like, clear breaking in band dispersion or band bending behavior was observed on the d_{xy} band, indicating an opening of the SDW gap on the d_{xy} h-pocket. In contrast, in the CSDW phase of $Sr_{0.64}Na_{0.36}Fe_2As_2$, the band bending behavior was observed on the $d_{xz,yz}$ bands, indicating a gap opening on the $d_{xz,yz}$ h-pockets. It should be noted that the $d_{xz,yz}$ bands exhibit a $\sim$ 30 meV SDW gap at E_F only in the CSDW phase.[31] No gap was observed on the $d_{xz,yz}$ bands in the SSDW phase near the CSDW phase boundary (temperature slightly higher than the CSDW transition temperature).[31] Thereby, the SDW gap opening on the $d_{xz,yz}$ bands could be viewed as a distinct characteristic of the CSDW phase.

In addition to the SDW gap, two hole-like bands with similar dispersions were observed at $k_x =\sim -0.7$ Å^{-1} [Figs. 1(d), 1(f), 1(h), and 1(j)]. According to band calculations, the d_{xz} and d_{yz} bands disperse along the k_y and k_x directions, respectively.[33–35] When the system is C4 symmetric in the CSDW phase, the dispersions of the d_{xz} and d_{yz} bands are identical. In this case, one sharp band representing the degenerate $d_{xz,yz}$ bands (red and green dashed lines) can be observed at $k_x =\sim -0.7$ Å^{-1} [Figs. 1(h) and 1(j)]. One could also observe a broad distribution of spectral weight at higher binding energy. It represents the d_{xy} band (blue broad line) that is less coherent than the $d_{xz,yz}$ bands.[36] When the C4 symmetry is broken, the dispersions of the d_{xz} and d_{yz} bands be-

come different.[34–36] In this case, two sharp bands representing the energy separated d_{xz} and d_{yz} bands can be observed at $k_x = \sim -0.7$ Å^{-1} [Figs. 1(d) and 1(f)]. While the d_{yz} band (green line) disperses near E_F, the d_{xz} band (red line) and d_{xy} band (blue broad line) disperse at higher binding energy. Such energy splitting of the d_{xz} and d_{yz} bands has been widely observed in the nematic phase of Fe-HTS.[29,31,34,35] Therefore, the lifting of energy degeneracy between the d_{xz} and d_{yz} bands could be viewed as an electronic structure indicator of the C4 symmetry breaking. It should be noted that here we only show the band dispersion along the k_x direction. However, due to the existence of twinned domains in samples with perpendicular directions, both the original d_{yz} band and the d_{xz} band projected from the 90°-rotated domains can be observed simultaneously along the k_x direction.[29,31,34,35] When the sample is detwinned, for example, by applying uniaxial strain, only the d_{yz} band is observable along the k_x direction near $k_x = \sim -0.7$ Å^{-1}.[29,30,34,35]

3.2. Alkali-metal deposition

After clarifying the characteristics of the electronic structure, we performed doping control on the C4 magnetic phase. Figure 2 shows the evolution of Fermi surface and band dispersions with increasing the alkali-metal deposition. We use Dn ($n = 0, 1, 2, \ldots$) to denote the deposition sequence. As shown in Figs. 2(a)–2(c), the surface deposition of lithium introduces electrons into the system: the h-pockets shrink and the e-pockets expand. The size of the e-pockets is more comparable to that of the $d_{xz,yz}$ h-pockets in the D0 sample. But in the D7 sample, the size of the e-pockets becomes more matched with the size of the d_{xy} h-pocket. Meanwhile, the relative intensity between the d_{xy} and $d_{xz,yz}$ h-pockets reverses with electron doping. The $d_{xz,yz}$ h-pockets exhibit lower (higher) photoemission intensity than the d_{xy} h-pocket in D0 (D7) samples. Such redistribution of photoemission intensity on the h-pockets indicates a switching of orbital selectivity of the SDW gap. As shown in Fig. 2(d), the d_{xy} band crosses E_F in the D0 sample but exhibits a clear band bending behavior in the D7 sample. In addition to the change of the SDW gap, two sharp band dispersions could be observed at $k_x = \sim -0.7$ Å^{-1} in the D7 sample [Figs. 2(d) and 2(e)], resembling the band dispersion in $SrFe_2As_2$ [Fig. 1(d)]. They represent the energy separated d_{xz} and d_{yz} bands, indicating that the symmetry of the system changes from C4 to C2. All the above phenomena consistently show that the alkali-metal deposition drives a transition of the system from C4 to C2 magnetic phase.

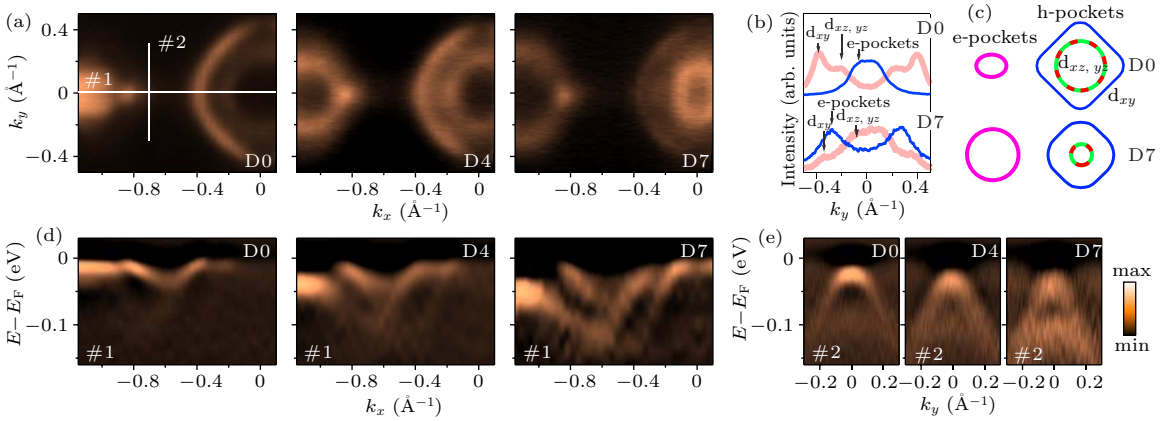


Fig. 2. Evolution of electronic structure in $Sr_{0.64}Na_{0.36}Fe_2As_2$ tuned via alkali-metal deposition. (a) Doping dependence of the photoemission intensity mapping taken at E_F in $Sr_{0.64}Na_{0.36}Fe_2As_2$. We use D$n$ ($n = 0, 1, 2, \ldots$) to denote the deposition sequence. (b) The momentum distribution curves taken across the h-pockets along the $k_x = 0$ Å^{-1} (red thick lines) and across the e-pockets along the $k_x = \sim -1.08$ Å^{-1} (blue thin lines) directions at D0 and D7. The Fermi crossings of the h- and e-pockets are highlighted using black arrows. (c) Schematic drawing of the doping dependence of the Fermi surface. (d) and (e) Doping dependence of the second derivative images of the energy momentum cuts taken along #1 and #2 directions. The cut directions are illustrated using the white solid lines in panel (a). The data were measured at 15 K.

We then characterized the SDW gap on the $d_{xz,yz}$ bands with high energy resolution. Figure 3 shows the symmetrized spectra taken at different doping levels. It should be noted that the symmetrization of spectra is not rigorous here, due to the presence of background and the fact that the spectral function of the SDW phase is not strictly particle-hole symmetric.[37] Nevertheless, as a common method for the gap analysis of the charge density wave and SDW phases, the symmetrization method effectively demonstrates the presence of spectral weight suppression at E_F. As shown in Fig. 3(a), the d_{xy} band exhibits no gap, while a large gap (Δ) of approximately 30 meV was observed on the $d_{xz,yz}$ bands. This is consistent with our previous ARPES study on the C4 magnetic phase.[31] When deposited with alkali-metal, a zero-energy peak emerges in the D5 sample (highlighted with a red arrow). Its peak area increases with further doping. A zero-energy peak in the symmetrized spectrum represents a gapless electronic state. However, as shown in Figs. 3(b) and 3(c), instead of a gradual reduction of the SDW gap to zero, the zero-energy peak emerges suddenly at E_F and coexists with the gapped state. The coexistence of the zero-energy peak and the peaks at 30 meV binding energy is consistent with a phase

separation behavior of a first-order phase transition. With increasing doping, part of the gapped state transits into a gapless state. The gapped and gapless states coexist in the system during the transition process.

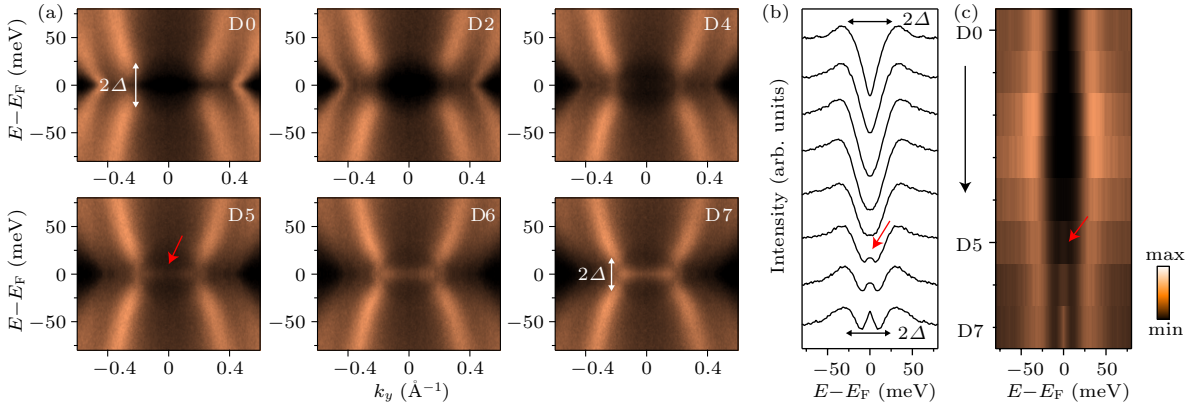


Fig. 3. Doping dependence of the SDW gap on the $d_{xz,yz}$ bands. (a) Doping dependence of the symmetrized images of the energy momentum cuts taken along the $k_x = 0$ Å^{-1} direction. We use Dn ($n = 0, 1, 2, \ldots$) to denote the deposition sequence. (b) Doping dependence of the symmetrized energy-distribution curves (EDCs) integrated in a [0, 0.3 Å^{-1}] momentum window. (c) Merged image of the symmetrized EDCs in panel (b). The data were measured at 15 K.

3.3. Uniaxial strain

Uniaxial tensile and compressive strains naturally break the C4 rotational symmetry of materials. According to previous studies, strong nematic fluctuations exist in wide doping and temperature ranges in the phase diagram of Fe-HTS.[28,38] As a result, the nematic order can be induced by applying uniaxial strain. Strain-induced nematic order has been observed in various Fe-HTS systems.[30,39,40] Figure 4 shows the Fermi surfaces and band dispersions measured under tensile and compressive strains, respectively. We use the voltage of the piezoelectric ceramic stacks (V_{pzt}) to show the magnitude of uniaxial strain. As discussed in previous sections, the energy separation between the d_{xz} and d_{yz} bands serves as a sensitive indicator of the C4 symmetry breaking in Fe-HTS. Here, due to the limitation of the matrix element effects of our experimental geometry, we only focused on the d_{yz} band dispersion along the k_x direction. As shown in Figs. 4(a)–4(d), the d_{yz} band shifts up under tensile strain resulting in an emergence of a bright intensity spot (highlighted by white arrows) in the Fermi surface mapping near the e-pockets. In contrast, the d_{yz} band shifts down under compressive strain leading to a decline of photoemission intensity of the bright spot. This phenomenon is consistent with previous ARPES studies on uniaxially strained $FeSe_{0.9}S_{0.1}$ and $Ba_{1-x}K_xFe_2As_2$,[29,30] indicating that the C4 rotational symmetry of the electronic structure is broken under tensile and compressive strains. The strain-induced energy difference of the d_{yz} band could be characterized by comparing the EDCs taken at $k_x = -0.7$ Å^{-1} with a V_{pzt} of −350 V and 300 V [Fig. 4(b)]. The energy difference is estimated to be around 20 meV, which could be viewed as a characteristic energy scale of the nematic order ($E_{nematic}$) induced by uniaxial strain. Similar strain-induced nematic order was consistently observed in another sample (sample #2) [Figs. 4(e)–4(h)]. In sample #2, a tiny amount of lithium (∼ 60 s deposition time) was deposited on the sample surface. Such a small amount of lithium could suppress the surface polarization effect without

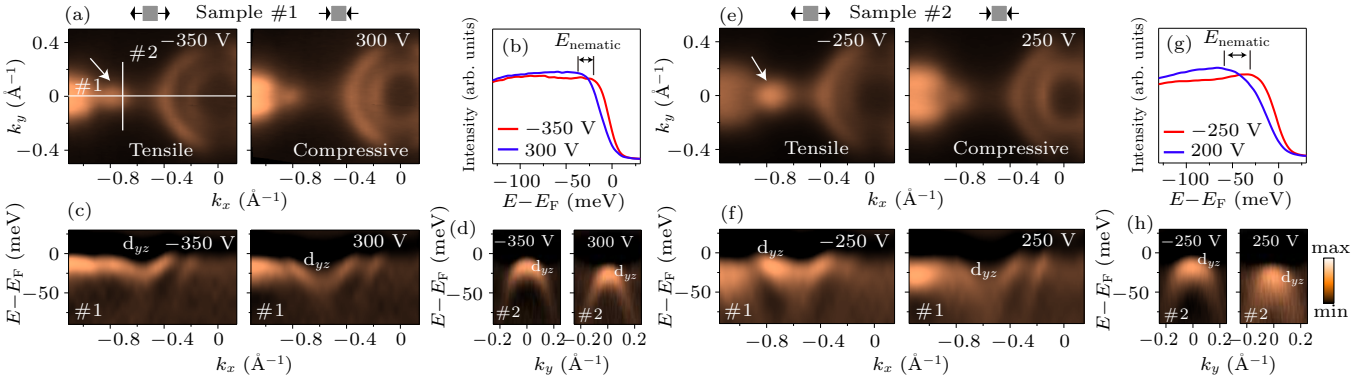


Fig. 4. Electronic structures of $Sr_{0.64}Na_{0.36}Fe_2As_2$ tuned via the tensile and compressive strains. (a) Photoemission intensity mapping at E_F taken in sample #1 under tensile and compressive strains. We use the voltage of the piezoelectric ceramic stacks (V_{pzt}) to show the magnitude of uniaxial strain. Negative and positive voltages represent the tensile and compressive strains, respectively. (b) EDCs extracted at $k_x = -0.7$ Å^{-1} and $k_y = 0$ Å^{-1} under tensile (−350 V) and compressive (300 V) strains. (c) and (d) Second derivative images of the energy momentum cuts taken along the #1 and #2 directions under tensile (−350 V) and compressive (300 V) strains. The cut directions are illustrated using white solid lines in panel (a). (e)–(h) are the same as (a)–(d), but taken in sample #2 with a tiny amount of lithium surface deposition. The data were measured at 45 K.

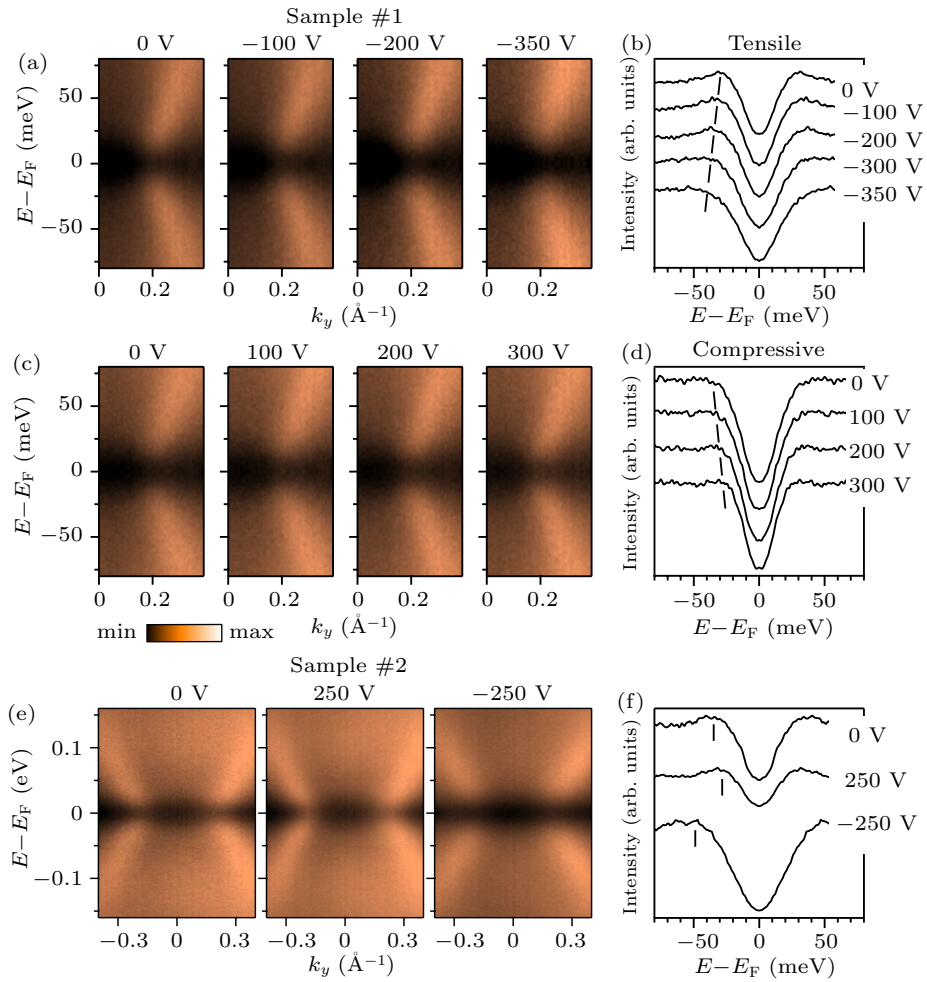


Fig. 5. Strain-dependence of the SDW gap on the $d_{xz,yz}$ bands. (a) Strain-dependence of the symmetrized images of the energy momentum cuts taken along the $k_x = 0$ Å^{-1} direction in sample #1 under tensile strain. We use V_{pzt} to show the magnitude of uniaxial strain. (b) Strain-dependence of the symmetrized EDCs taken at the Fermi crossings of the $d_{xz,yz}$ bands in sample #1 under tensile strain. (c) and (d) are the same as (a) and (b), but taken in sample #1 under compressive strain. (e) and (f) are the same as (a) and (b), but taken in sample #2 under tensile and compressive strains. The data were measured at 45 K.

affecting the C4 magnetic phase.[32] The strain-induced shift of the d_{yz} band is more pronounced in sample #2. The strain-induced $E_{nematic}$ reaches around 30 meV [Fig. 4(g)]. If we use the ratio of the nematic transition temperature ($T_{nematic}$) to the $E_{nematic}$ measured in $FeSe_{0.9}S_{0.1}$,[29] the calculated $T_{nematic}$ of the strain-induced nematic order in $Sr_{0.64}Na_{0.36}Fe_2As_2$ is $\sim$ 50–60 K.

We confirmed that a nematic order with a 20-30 meV energy scale was induced by uniaxial strain in $Sr_{0.64}Na_{0.36}Fe_2As_2$. We then studied the change of magnetic order by measuring the strain dependence of the SDW gap on the $d_{xz,yz}$ bands with high energy resolution. As shown in Figs. 5(a) and 5(b), the gap on the $d_{xz,yz}$ bands gradually increases with increasing tensile strain. The gap expands to around 40 meV at a V_{pzt} of −350 V. In contrast, the gap gradually decreases to $\sim$ 25 meV with increasing compressive strain [Figs. 5(c) and 5(d)]. The strain dependence of the SDW gap was consistently observed in sample #2 [Figs. 5(e) and 5(f)]. The energy scale of the strain-induced gap modulation is around $\sim$ 15–20 meV. The signature of the gapless state as manifested by the zero-energy peak was not observed in either tensile or compressively strained samples in our strain tuning range.

4. Discussion

Figure 6 summarizes our results. We first discuss the evolution of magnetic order with doping. We attribute the zero-energy peak to the SSDW phase with C2 symmetry. We made this attribution based on the following reasons. (i) The alkali-metal deposition dopes electrons into the system driving the electronic state of $Sr_{0.64}Na_{0.36}Fe_2As_2$ toward the electronic state in its parent compound $SrFe_2As_2$. Therefore, a doping induced CSDW-to-SSDW transition is expected. (ii) The closing of the SDW gap on the $d_{xz,yz}$ h-pockets and the observation of energy splitting of the $d_{xz,yz}$ bands at $k_x = -0.7$ Å^{-1} are consistent with the characteristics of the SSDW phase. (iii) Both experimental and theoretical studies have shown that the CSDW-to-SSDW transition is a first-order transition due to the reorientation of magnetic moments from out-of-plane to

in-plane direction.[9–12,17,31] This is consistent with the phase separation phenomena we observed here. Part of the CSDW phase starts to transition into the SSDW phase at around 75 s deposition time. The two phases then coexist in the system, while the proportion of the SSDW phase gradually increases with increasing electron doping. The coexistence of CSDW and SSDW phases also explains our Fermi surface mapping taken in the D7 sample [Fig. 2(a)]. The d_{xy} h-pocket is gapless in the CSDW phase. Therefore, the photoemission signal originated from the residual CSDW phase leads to the observation of the sharp d_{xy} h-pocket in the Fermi surface mapping of the D7 sample.

Unlike the doping induced CSDW-to-SSDW transition, the response of the C4 magnetic phase to uniaxial strain is counterintuitive. We confirmed that the uniaxial strain breaks the C4 symmetry of the system. A nematic order with an energy scale of $\sim$ 20–30 meV is induced. Considering the presence of finite coupling among orbitals, lattice, and magnetism, the magnetic phase should be also C2 symmetric under the tensile and compressive strains. Note that, the C4 CSDW phase can only transition into the C2 SSDW phase via a first-order phase transition.[9–12,17,31] However, we observed a continuous modulation of the SDW gap by uniaxial strain. There is no signature of a first-order transition. Neither the phase separation behavior nor the zero-energy peak has been observed. We then considered two possible scenarios. On the one hand, according to theories, the CSDW phase could couple with an out-of-plane SVC (SVC$_\perp$) and SSDW phases so that it could break the C4 symmetry continuously via a second-order transition.[17] In this case, the strain-dependence of SDW gap in Fig. 6(d) could be attributed to a gap anisotropy. With the development of C2 magnetic order, the SDW gap increases along one direction and decreases along the perpendicular direction. Because the magnetic domain rotates 90° from tensile to compressively strained samples, we observe the increase and decrease of the SDW gap under tensile and compressive strains. However, there is no experimental evidence for the existence of a SVC$_\perp$ phase in Fe-HTS so far. Moreover, the Fermi surface mappings of our strained samples show a uniform angular distribution of photoemission intensity on the $d_{xz,yz}$ h-pockets, which contradicts to the presence of strong gap anisotropy. On the other hand, a more plausible scenario is that similar to the doped case, part of the CSDW phase transitions into a SSDW phase through a first-order transition. But the proportion of the SSDW phase is too low to be detected by our gap measurements. In this case, our measurements of the strain-dependence of the SDW gap reflect the strength of the CSDW phase. If only the in-plane effects of tensile and compressive strains are considered, their impacts on the electronic state should be identical, differing only by a 90° rotation. However, our data observed that the CSDW phase is enhanced (weakened) under tensile (compressive) strain. To explain this asymmetry, we need to consider the out-of-plane effects of tensile and compressive strains. Tensile strain causes a compression of lattice along the out-of-plane direction, while compressive strain causes an expansion of lattice along the out-of-plane direction. It is possible that the strain-dependence of the SDW gap observed in Fig. 6(d) reflects the sensitivity of the CSDW phase to the tuning of the lattice along the out-of-plane direction. Further experiments involving uniaxial strain applied along the c-axis may be required to verify this proposal.

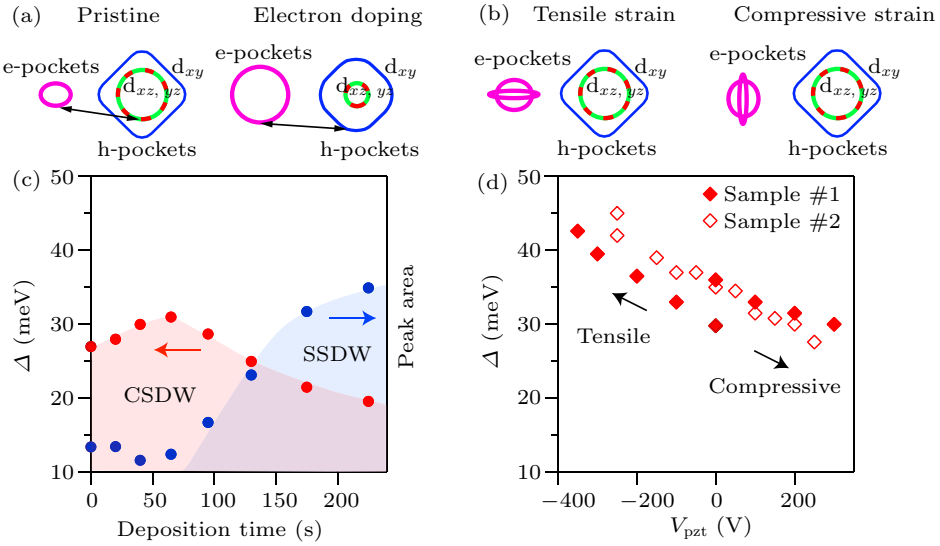


Fig. 6. Response of the CSDW phase to doping and uniaxial strain. (a) and (b) Schematic drawing of the change of Fermi pockets with electron doping and uniaxial strain. For the case of uniaxial strain, only the anisotropy of e-pockets is considered. The anisotropic e-pockets were draw according to previous ARPES studies on the nematic phase.[29,31,34,35] (c) Doping dependence of the SDW gap (red circles) and the peak area of the zero-energy peak (blue circles). (d) Strain dependence of the SDW gap extracted from the data taken in samples #1 (solid diamonds) and #2 (hollow diamonds).

Nevertheless, in either case, the small magnitude of the gap variation (approximately 15 meV) and the absence of a gapless state both indicate that the C4 magnetic phase exhibits a certain degree of robustness under uniaxial strain. The C4 magnetic phase coexists with the strain-induced nematic order in the entire strain tuning range of our experiment in $Sr_{0.64}Na_{0.36}Fe_2As_2$. Such robustness of the C4 magnetic phase suggests that the nematic order exhibits no intermediate correlation with the magnetic phase. This falsifies the previous view of the relation between nematic and magnetic orders that the nematic order is the precursor order of the magnetic order.[23,24] Our results imply that the nematic and magnetic fluctuations in Fe-HTS have different origins.

Next, we discuss the mechanism of magnetic fluctuations in Fe-HTS. First, as shown in Fig. 6(b), the e-pockets become strongly anisotropic due to the formation of the nematic order under uniaxial strain. In this case, the nesting of the Fermi surface would choose only one direction $(0, \pi)$ or $(\pi, 0)$. If the magnetic fluctuations purely originate from the Fermi surface instability, the C4 magnetic phase should be strongly suppressed in both tensile and compressively strained samples. This is inconsistent with our observation. Furthermore, while the Fermi surface became anisotropic under uniaxial strain, an approximately 10 meV enhancement of the CSDW gap was observed. Therefore, our results suggest that the magnetic fluctuations cannot originate purely from the Fermi surface instability of itinerant electrons. High energy interactions such as Hund's interactions or exchange interactions need to be considered.[20] Second, as shown in Fig. 6(a), the nesting condition switches from e-pockets-$d_{xz,yz}$ h-pockets to e-pockets-d_{xy} h-pockets with electron doping. Consistently, the orbital selectivity of the SDW gap also switches. This suggests that the orbital selectivity of Fermi surface nesting plays a crucial role in determining the orientation of magnetic moments or magnetic configuration. This is also supported by theoretical calculations.[25,41] The nesting of Fermi pockets between e-pockets and d_{xy} h-pocket favors the SSDW phase. This explains why the SSDW phase was not found in LiFeAs and FeSe where there is no nesting condition for the d_{xy} h-pocket. In contrast, the CSDW phase was only found in hole-doped FeAs compounds, which means that the CSDW phase could be stabilized by the nesting between the e-pockets and the $d_{xz,yz}$ h-pockets. This also explains the robustness of the CSDW phase under uniaxial strain. The uniaxial strain only induces anisotropy in the e-pockets. The nesting of Fermi pockets between the e-pockets and the $d_{xz,yz}$ h-pockets remains intact under uniaxial strain.

5. Conclusion

In summary, we applied doping and uniaxial strain tuning to the C4 magnetic phase in Fe-HTS. Using ARPES, we characterized the evolution of the Fermi surface and the SDW gap. We found that the electron doping drives a first-order CSDW-to-SSDW transition, while no such transition was observed in the uniaxially strained samples. On the one hand, our results suggest that the nematic order exhibits no close correlation with the magnetic order in Fe-HTS. They may have different origins. Experimental studies on Fe-HTS have found that both the nematic and magnetic fluctuations exist in a wide region of the phase diagram.[3] Both fluctuations have been proposed to contribute to the superconducting pairing interactions. Therefore, in order to explain the complex superconducting states of Fe-HTS, the cooperative or competitive contributions from both the nematic and magnetic fluctuations may need to be considered. On the other hand, our results show that the orbital selectivity of Fermi surface nesting plays a crucial role in determining the moment orientation or magnetic configuration of Fe-HTS, which confirms the role of itinerant electrons in mediating the magnetic fluctuations in Fe-HTS. Meanwhile, the existence of two nesting channels on the Fermi surface with different orbital characters may be related to the strong orbital selectivity of superconductivity found in Fe-HTS. In most Fe-HTS, the superconducting gap on the $d_{xz,yz}$ bands is larger than that on the d_{xy} band.[3,31] Such orbital selectivity of superconductivity is more consistent with the orbital selectivity of the SDW gap in the CSDW phase than that of the SSDW phase.[31] It is intriguing to further study how the magnetic fluctuations originating from magnetic orders with different symmetries (C2 and C4) play roles in mediating the superconducting pairing in Fe-HTS.

Acknowledgements

This work was supported by the National Natural Science Foundation of China (Grant No. 12474129) and the National Key Research and Development Program of China (Grant No. 2022YFA1403502).

References

[1] Keimer B, Kivelson S A, Norman M R, Uchida S and Zaanen J 2015 *Nature* **518** 179
[2] Wang F and Lee D H 2011 *Science* **332** 200
[3] Fernandes R M, Coldea A I, Ding H, Fisher I R, Hirschfeld P J and Kotliar G 2022 *Nature* **601** 35
[4] Dai P C 2015 *Rev. Mod. Phys.* **87** 855
[5] Bao W, Qiu Y, Huang Q, Green M A, Zajdel P, Fitzsimmons M R, Zhernenkov M, Chang S, Fang M H, Qian B, Vehstedt E K, Yang J H, Pham H M, Spinu L and Mao Z Q 2009 *Phys. Rev. Lett.* **102** 247001
[6] Wang M, Wang M Y, Li G N, *et al*. 2011 *Phys. Rev. B* **84** 094504
[7] Huang Q, Qiu Y, Bao W, Green M A, Lynn J W, Gasparovic Y C, Wu T, Wu G and Chen X H 2008 *Phys. Rev. Lett.* **101** 257003
[8] Cruz C, Huang Q, Lynn J W, Li J Y, Ratcliff II W, Zarestky J L, Mook H A, Chen G F, Luo J L, Wang N L and Dai P C 2008 *Nature* **453** 899
[9] Avci S, Chmaissem O, Allred J M, Rosenkranz S, Eremin I, Chubukov A V, Bugaris D E, Chung D Y, Kanatzidis M G, Castellan J P, Schlueter J A, Claus H, Khalyavin D D, Manuel P, Daoud-Aladine A and Osborn R 2014 *Nat. Commun.* **5** 3845
[10] Böhmer A E, Hardy F, Wang L, Wolf T, Schweiss P and Meingast C 2015 *Nat. Commun.* **6** 7911

[11] Allred J M, Taddei K M, Bugaris D E, Krogstad M J, Lapidus S H, Chung D Y, Claus H, Kanatzidis M G, Brown D E, Kang J, Fernandes R M, Eremin I, Rosenkranz S, Chmaissem O and Osborn R 2016 *Nat. Phys.* **12** 493

[12] Taddei K M, Allred J M, Bugaris D E, Lapidus S, Krogstad M J, Stadel R, Claus H, Chung D Y, Kanatzidis M G, Rosenkranz S, Osborn R and Chmaissem O 2016 *Phys. Rev. B* **93** 134510

[13] Meier W R, Ding Q P, Kreyssig A, Bud'ko S L, Sapkota A, Kothapalli K, Borisov V, Valentí R, Batista C D, Orth P P, Fernandes R M, Goldman A I, Furukawa Y, Böhmer A E and Canfield P C 2018 *npj. Quant. Mater.* **3** 5

[14] Kreyssig A, Wilde J M, Böhmer A E, Tian W, Meier W R, Li B, Ueland B G, Xu M Y, Bud'ko S L, Canfield P C, McQueeney R J and Goldman A I 2018 *Phys. Rev. B* **97** 224521

[15] Wang L, He M, Scherer D D, Hardy F, Schweiss P, Wolf T, Merz M, Andersen B M and Meingast C 2019 *J. Phys. Soc. Jpn.* **88** 104710

[16] Sheveleva E, Xu B, Marsik P, Lyzwa F, Mallett B P P, Willa K, Meingast C, Wolf Th, Shevtsova T, Pashkevich Y G and Bernhard C 2020 *Phys. Rev. B* **101** 224515

[17] Christensen M H, Orth P P, Andersen B M and Fernandes R M 2018 *Phys. Rev. B* **98** 014523

[18] Christensen M H, Andersen B M and Kotetes P 2018 *Phys. Rev. X* **8** 041022

[19] Fang C, Yao H, Tsai W F, Hu J P and Kivelson S A 2008 *Phys. Rev. B* **77** 224509

[20] Dai P C, Hu J P and Dagotto E 2012 *Nat. Phys.* **8** 709

[21] Hirschfeld P J, Korshunov M M and Mazin I I 2011 *Rep. Prog. Phys.* **74** 124508

[22] Fernandes R M, Chubukov A V and Schmalian J 2014 *Nat. Phys.* **10** 97

[23] Lee C C, Yin W G and Ku W 2009 *Phys. Rev. Lett.* **103** 267001

[24] Chubukov A V, Khodas M and Fernandes R M 2016 *Phys. Rev. X* **6** 041045

[25] Onari S and Kontani H 2022 *Front. Phys.* **10** 915619

[26] Seo J J, Kim B Y, Kim B S, Jeong J K, Ok J M, Kim J S, Denlinger J D, Mo S K, Kim C and Kim Y K 2016 *Nat. Commun.* **7** 11116

[27] Han T T, Chen L, Cai C, Wang Z G, Wang Y D, Xin Z M and Zhang Y 2021 *Phys. Rev. Lett.* **126** 106602

[28] Chu J H, Kuo H H, Analytis J G and Fisher I R 2012 *Science* **337** 710

[29] Cai C, Han T T, Wang Z G, Chen L, Wang Y D, Xin Z M, Ma M W, Li Y and Zhang Y 2020 *Phys. Rev. B* **101** 180501

[30] Chen L, Han T T, Cai C, Wang Z G, Wang Y D, Xin Z M and Zhang Y 2021 *Phys. Rev. B* **104** L060502

[31] Han T T, Chen L, Cai C, Wang Y D, Wang Z G, Xin Z M and Zhang Y 2020 *Phys. Rev. Lett.* **124** 247002

[32] Xin Z M, Wang Y D, Cai C, Wang Z G, Chen L, Han T T and Zhang Y 2021 *Commun. Phys.* **4** 31

[33] Fernandes R M and Chubukov A V 2017 *Rep. Prog. Phys.* **80** 014503

[34] Yi M, Zhang Y, Shen Z X and Lu D H 2017 *npj. Quant. Mater.* **2** 57

[35] Böhmer A E, Chu J H, Lederer S and Yi M 2022 *Nat. Phys.* **18** 1412

[36] Pfau H, Chen S D, Hashimoto M, Gauthier N, Rotundu C R, Palmstrom J C, Fisher I R, Mo S K, Shen Z X and Lu D 2021 *Phys. Rev. B* **103** 165136

[37] Norman M R, Randeria M, Ding H and Campuzano J C 1998 *Phys. Rev. B* **57** R11093

[38] Kuo H H, Chu J H, Palmstrom J C, Kivelson S A and Fisher I R 2016 *Science* **352** 958

[39] Yim C M, Trainer C, Aluru R, Chi S, Hardy W N, Liang R X, Bonn D and Wahl P 2018 *Nat. Commun.* **9** 2602

[40] Kushnirenko Y S, Evtushinsky D V, Kim T K, Morozov I, Harnagea L, Wurmehl S, Aswartham S, Büchner B, Chubukov A V and Borisenko S V 2020 *Phys. Rev. B* **102** 184502

[41] Christensen M H, Scherer D D, Kotetes P and Andersen B M 2017 *Phys. Rev. B* **96** 014523